Macromolecules

pubs.acs.org/Macromolecules Article

Decoupling Multiple Relaxation Modes: Composition and Distribution of Terminal Relaxation Time in Associative Polymers

Xiang Cui,[+] Yulin Luo,[+] Yuliang Yang, and Ping Tang*

Cite This: *Macromolecules* 2025, 58, 1898−1911 Read Online

ACCESS | Metrics & More | Article Recommendations | Supporting Information

ABSTRACT: The distinctive rheological behavior of associative polymers (APs) is commonly attributed to the supramolecular interactions between stickers, where transient bonds are continually forming and breaking. This ongoing disruption and reconstruction significantly extend the terminal relaxation time, endowing APs with properties similar to those of entangled polymers. Based on the fundamental sticky Rouse model (SRM), the terminal relaxation of APs can be understood as a result of a combination of strand motion and associative interactions. However, this explanation may be overly simplistic. The presence of multiple relaxation modes arising from a broader range of molecular processes introduces complexity, and their individual contributions to the terminal relaxation time remain uncertain. In this work, we focus on decoupling these multiple relaxation modes. Our findings reveal that, beyond strand motion and associative interactions, the terminal relaxation time is also influenced by factors such as the loss of cross-links, reassociation dynamics, and small molecule reactants. Furthermore, the difference between the activation energy required for strand motion and the magnitude of reaction kinetic activation energy between stickers plays a crucial role in determining the distribution of the terminal relaxation time. We believe that this work offers significant insights into the linear viscoelasticity (LVE) of APs.

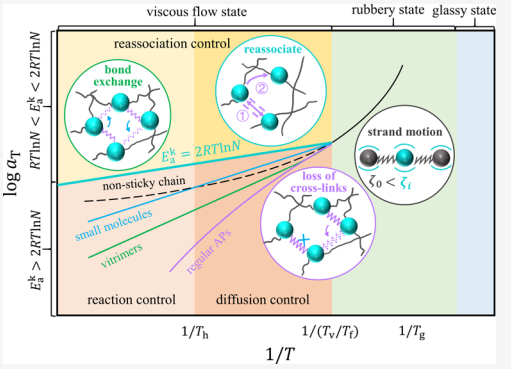

1. INTRODUCTION

The introduction of interchain interactions significantly changes the dynamics of polymers. These interactions involve reversible covalent bonds,[1] van der Waals interactions,[2−4] $\pi-\pi$ stacking interactions,[5,6] hydrogen-bonding interactions,[7] ionic interactions.[8−13] Polymers with these interactions, known as associative polymers (APs), are notable for their unique rheological behavior. APs can frequently dissociate and associate under specific conditions, forming a dynamic cross-linked network. For regular APs like dissociative covalent adaptable networks (Diss-CANs), the loss of cross-linking density introduces an additional relaxation mode. Conversely, associative CANs or vitrimers,[14] undergo bond exchange reactions (BERs) that maintain the cross-linking density, resulting in distinct viscoelastic properties.

Understanding the linear viscoelasticity (LVE) of APs requires extensive researches into their molecular structure and kinetics. Experimental studies have extensively explored the viscoelastic behavior of APs, focusing on specific associative interactions and the modulation of viscoelastic properties.[15−20] Notable examples include UPy-functionalized poly(*n*-butyl acrylate) (PnBA-UPy) for hydrogen bonding, deprotonated sulfonated polystyrene (SPS-Na) for ionic interactions, and hydrophobically modified ethoxylated urethane (HEUR) for hydrophilic−hydrophobic interactions. Watanabe's group[21−23] investigated the concentration dependence of HEUR's rheological properties, and Chen's group[24−26] studied the LVE of SPS ionomers and developed the reversible gelation model.[8]

Theoretical frameworks for APs originated from the phenomenological sticky theory,[27] leading to models like the reversible gelation model,[28] sticky Rouse model,[29] and sticky reptation model.[30] The sticky Rouse model (SRM), assuming mean-field interactions, treats associative interactions as larger frictions on the stickers rather than the usual segments. Our group[31] expanded this model and introduced association interactions to solve Rouse dynamics equations, decoupling fast chain relaxation from slow viscous relaxation and validating it through molecular simulations.[32] Subsequently, we further extended it to a dual network system.[33] To overcome the limitations of the mean-field assumptions, molecular simulation methods were developed with new algorithms and potentials. Hybrid Monte Carlo and Molecular Dynamics (hybrid MC/MD) algorithms have been developed to describe the associative interactions in APs. Hoy and Fredrickson[34] used hybrid MC/MD algorithm to investigate detailed

Received: September 27, 2024
Revised: January 26, 2025
Accepted: February 3, 2025
Published: February 7, 2025

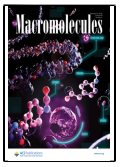

https://doi.org/10.1021/acs.macromol.4c02349
Macromolecules 2025, 58, 1898−1911

chemical dynamics, identifying kinetically and diffusion-limited association behaviors. Building on this method,[34] Wu et al.[35] and Perego et al.[36,37] examined the effects of temperature and activation energy on BERs in vitrimers, revealing how BERs rates influenced the molecular diffusion and relaxation dynamics. Recently, Xia et al. used a coarse-grained MD/MC method to study the topological structural changes, microscopic dynamics, and LVE of unentangled side-chain-linked vitrimers. The simulation results show quantitative agreement with single-chain SRM predictions for unentangled vitrimers with a fast bond-exchange rate.[38] Extending this approach, they simulated vitrimers with short chains, high bond-exchange energy barriers, and high cross-linker concentrations, revealing reptation-like dynamics typically associated with highly entangled polymer systems.[39]

However, the hybrid MC/MD method may violate potential energy conservation. To address this, Sciortino[40] introduced a three-body potential that allowed for BERs within standard MD, enabling the simulation of stress relaxation,[41] fragility,[42] dynamics,[43] and self-healing[44] of vitrimers. Expanding on this, Zhao et al.[45] discovered through the three-body potential that vitrimers achieved optimal mechanical properties at an intermediate energy barrier. We speculate that such nonbonded interactions may not be suitable for exploring nonlinear viscoelasticity. Our group[46] recently designed a hybrid MC/MD algorithm to simulate BERs in vitrimers with controllable activation energy, allowing us to compare both the linear and nonlinear viscoelasticities of APs.

Most previous research has focused on the overall terminal relaxation rather than the multiple relaxation modes within APs. Some studies observed coupling among relaxation modes, such as the integration of chain dynamics and sticker dissociation time scales by Zhang et al.[47] The interactions between stickers impede segment relaxation, making chain dynamics sensitive to interaction energy. Perego et al.[37] noted that neglecting activation energy led to the chemical reaction proceeding at the maximum rate, causing an overlap of terminal relaxation with Rouse relaxation in the master curve. This is a prevalent phenomenon in APs and poses a considerable challenge for rheological analysis. Watanabe et al.[48] and Matsumiya et al.[49] found that faster reaction rates coupled with segmental motion, creating new relaxation modes. Olsen's group[50,51] explored walking and hopping diffusion in APs, revealing a multiscale self-diffusion mechanism stemming from the interplay between segmental motion and associative interactions. Similarly, Wu et al.[52,53] found that sticker lifetimes significantly exceed the strand Rouse time in vitrimers based on dioxaborolane metathesis, indicating a reaction-controlled rather than diffusion-influenced relaxation, and it is generally believed that a broad temperature window facilitated identifying the dynamic mode that governs terminal relaxation of vitrimers.[54] Furthermore, Zhao et al.[55] revealed the bond swap energy barrier and temperature dependence of multiscale dynamic behaviors in vitrimer. Obviously, decoupling various relaxation modes is crucial for a thorough understanding of the LVE of APs.

In regular APs, associative reactions will inevitably lead to specific situations, such as the loss of cross-linking density and reassociation between stickers. Our previous research[46] found that the additional relaxation due to loss of cross-links in regular APs was reflected in the prefactor of terminal relaxation time, which emerged from the decoupling of additional relaxation. Besides, recent researches highlighted the significance of sticker reassociation.[56,57] According to the bond lifetime renormalization model,[56] an open sticker can reassociate with its previous partner multiple times before associating with a new partner, as validated by a combination of dielectric and rheology analyses.[58] Shanbhag and Ricarte[59] further affirmed the scaling relations in the model based on fractional Brownian simulations. Analogously, drawing on the concept of compact random walks, Gold et al.[60] reconfirmed that additional relaxation in experiments could be attributed to reassociation.

In summary, despite significant efforts, the coexistence and coupling of multiple relaxation modes in APs remain incompletely understood. There is a demand for a microscopic theory that considers multiple relaxation modes in APs and separates their contributions on the terminal relaxation. Inspired by earlier studies, we start with the sticky Rouse model, focusing on the source of the network relaxation and identifying deviations from theoretical results through molecular simulation. This leads us to propose that terminal relaxation of APs may comprise strand motion, association reaction, loss of cross-links and reassociation, while exhibiting a distribution. By employing theoretical frameworks and simulations, we aim to decouple these complex relaxation modes, providing a microscopic understanding of APs' viscoelastic behaviors and enhancing the theoretical foundation for integrating experimental observations with simulations.

2. THEORY AND SIMULATION METHOD

2.1. Sticky Rouse Model (SRM). The SRM, a single-chain model proposed simultaneously by Hansen and Shen,[61] Wang and DiMarzio,[62] and Stockmayer and Kennedy,[63] was originally developed to describe the LVE of block copolymers. Recently, we established that the SRM could be a robust framework for examining the LVE of APs. Its core concept simplifies coupled motions through effective friction.[31,32,46] To facilitate the understanding of subsequent calculations, the SRM is briefly reformulated in the following sections, with further details available in our previous work.[31]

For linear chains, there are N beads at positions $\mathbf{R}_{ij}$ with a friction coefficient of ζ_i and $N - 1$ springs with a spring coefficient of $k_i = 3k_BT/b^2$, where b is the Kuhn length. Assuming homogeneity, all friction coefficients and spring coefficients are the same, namely $\zeta_i = \zeta$ and $k_i = k$. According to Brownian motion, the equation of motion is

$$\dot{\mathbf{r}}_i + \sum_{j=1}^{N-1} C_{ij}\mathbf{r}_j = \mathbf{f}_i^B,\ i = 1, 2, ..., N \tag{1}$$

where $\dot{\mathbf{r}}_i$ represents the velocity of the ith bead, and the tridiagonal matrix $\mathbf{C}$ represents the connectivity of the chain. It is defined as $C_{ij} = (k/\zeta)A_{ij}$, where A_{ij} encodes the chain structure: $A_{ij} = 2$ for internal beads $(2 \le i \le N\text{-}1)$, $A_{ii} = 1$ for end beads ($i = 1$ and $i = N$), $A_{ij} = -1$ for adjacent beads ($i = j \pm 1$), and $A_{ij} = 0$ for other cases, respectively. $\mathbf{f}_i^B$ represents the random force acting on the bead i satisfying the fluctuation−dissipation correlation.

By calculating the eigenvalues of matrix $\mathbf{C}$, where $\lambda_i = 4(k/\zeta)\sin^2(i\pi/2N)$, we can extract the Rouse relaxation time spectrum through an inverse proportionality relationship: $\tau_i = 1/2\lambda_i = \zeta/(8k\sin^2(i\pi/2N))$. Thus, all physical properties related to linear viscoelasticity can be obtained. The relaxation modulus is

https://doi.org/10.1021/acs.macromol.4c02349
Macromolecules 2025, 58, 1898−1911

$$G(t) = \frac{G_N^0}{N}\sum_{i=1}^{N-1} e^{-t/\tau_i},\ G_N^0 = \rho k_B T \tag{2}$$

where G_N^0 and ρ represent the plateau modulus and the number density of cross-links, respectively.

For APs, the friction is not uniform across all beads, stickers exhibit higher frictions than regular beads, thus a more general matrix $\mathbf{C}$ is used:

$$\begin{aligned} C_{i,i-1} &= -k_{i-1}/\zeta_i \\ C_{i,i} &= k_i/\zeta_i + k_i/\zeta_{i+1} \\ C_{i,i+1} &= -k_{i+1}/\zeta_{i+1} \end{aligned} \tag{3}$$

The dynamics equation of the SRM can be derived by inserting the matrix $\mathbf{C}$ (eq 3) into eq 1. Compared with the Rouse model, a diagonal matrix Ξ is introduced to describe the friction of segments, with its diagonal elements ($\delta_i = \zeta_i/\zeta$) representing the relative friction coefficient of the ith segment. The association interaction is characterized by a larger friction force δ_i compared to regular beads, making the solution of the equations of motion (the eigenvalues of matrix $\mathbf{C}$) more challenging. While numerical solutions are feasible, it is preferable to use graph theory[31,33] methods to obtain an analytical solution.

2.2. Equilibrium Molecular Dynamics (EMD) Simulation. Similar to our previous work,[46] without incorporating bond angular potential, the coarse-grained Kremer-Grest (KG) bead−spring model is used to represent polymer networks.[64] We construct 500 chains of length $N = 50$ in a cubic periodic box with box length $L_i > 2\langle R_{ee}\rangle$ to prevent overlap and self-interaction between chains, where $\langle R_{ee}\rangle$ is the mean end-to-end distance. The length $N = 50$ is smaller than the entanglement length N_e, which ranges from $50 \le N_e \le 85$. The interaction energy between unbonded monomers employs the Lennard-Jones (LJ) truncated and shifted potential U_{LJ}:

$$U_{LJ}(r) = 4\varepsilon\left[\left(\frac{\sigma}{r}\right)^{12} - \left(\frac{\sigma}{r}\right)^{6} - \left(\frac{\sigma}{r_c}\right)^{12} + \left(\frac{\sigma}{r_c}\right)^{6}\right] \tag{4}$$

where r is the distance between monomers, and the cutoff radius $r_c = 2^{1/6}$ indicates purely repulsive interaction. All quantities are expressed in terms of LJ units: bead diameter σ, interbead interaction energy ε, and reduced time $\tau_{LJ} = \sqrt{m\sigma^2/\varepsilon}$, where m denotes the mass of an LJ bead. The number density of the LJ beads is $\rho = 0.85$. The finite extensible nonlinear elastic (FENE) potential is applied to describe the bonded interaction between beads:

$$U_{FENE}(r) = -\frac{1}{2}kR_0^2\ln[1 - (r/R_0)^2] \tag{5}$$

where the spring constant $k = 30$ and the maximum bond length $R_0 = 1.5$. Simulations are performed using LAMMPS[65] with the canonical ensemble (NVT), maintaining temperature with the Langevin thermostat. The velocity Verlet algorithm is employed to integrate Newton's equations of motion, utilizing a time step of $\delta t = 0.01$ (namely the real time step $(\delta t)^* = 0.01\tau_{LJ}$) at temperatures $T = 0.8$−1.6. The choice of time step has been validated to prevent chain crossing.

As shown in Figure S2 of the SI, each chain contains $N_s = 4$ stickers, evenly distributed at $N_i = 7,19,31,44$. To prevent phase separation, each sticker can bond only with another sticker. The premixed chains are cross-linked for 10^8 steps to form a fully cross-linked network with about 2.5% loops and no unreacted stickers. This fully cross-linked network serves as the initial state for both regular APs and vitrimers. Association reactions in APs can occur through either a dissociation-to-association process, which decreases the cross-linking density, or an association-to-dissociation process, which maintains the cross-linking density, as observed in vitrimers. These two types of chemical reactions are simulated using the hybrid MC/MD algorithm proposed by Hoy and Fredrickson,[34] and our previous work.[46] The details and differences between these two simulation methods are discussed in the Section S1 of the SI. After benchmarking, MC steps are performed every 100 MD time steps to effectively simulate chemical reactions while minimizing disruptions to the continuity of potential energy. The critical simulation parameter f_{MC} represents the fraction of stickers considered for exchange in each MC time step. Clearly, f_{MC} influences the kinetics of bond exchange reactions without altering the thermodynamics. Specifically, in a system with $f_{MC} = 0.5$, 50% of the stickers are randomly selected during each MC time step as candidates for chemical reactions. Although often overlooked, f_{MC} plays a significant role in the association dynamics between stickers and is crucial for accurately determining the terminal relaxation time (see Section 3.4). A more detailed explanation is provided in Section S2 of SI.

3. RESULTS AND DISCUSSIONS

3.1. Decoupling of Rouse Relaxation and Associative Interaction. The coupling of relaxation between segments and the network is widely observed in both experiments and simulations of APs, especially near the gelation point. This coupling is reflected in the indistinguishable relaxation modulus spectrum. For fully gelated APs, the SRM facilitates the direct decoupling of strand motion and associative interactions.[31] When the relative friction coefficient $\delta \gg 1$, the relaxation modulus $G(t)$ in the SRM can be simplified as follows:

$$G(t) = \frac{\nu k_B T}{N}\left[\sum_{p=N_s}^{N} \exp(-tp^2/\tau_R) + \sum_{p=1}^{N_s-1} \exp(-tp^2/\tau_s)\right] \tag{6}$$

here, $p = 1,2,\cdots,N$, represents the Rouse modes, ν denotes the number density of cross-links, while τ_R and τ_s represent the intrinsic Rouse relaxation time of the ideal chain without stickers and the terminal relaxation time, respectively. In this equation, the first summation accounts for the fast Rouse modes of the polymer chain, while the second summation represents the slow sticky modes arising from sticky friction. This decomposition clearly demonstrates that $G(t)$ is contributed by two parts: regular friction from Rouse motion and sticky friction from associative interactions, with the latter typically dominating the terminal relaxation.

Inspired by Ricarte's work,[66] we replicate and validate their calculations using both theoretical and simulation approaches to analyze the results from a decoupling perspective. Applying the single-chain model under the mean-field assumption, we use the SRM to calculate the stress relaxation moduli of vitrimers with a chain length of $N = 50$. The calculations for the SRM theory and molecular simulations are performed under the same conditions: $T = 0.8$∼1.6, and reaction kinetic activation energies $E_a^k = 2$∼10 (benchmarked by fitting simulation data with SRM theory, with corresponding $\delta =$

https://doi.org/10.1021/acs.macromol.4c02349
Macromolecules 2025, 58, 1898−1911

100~3000 as reported in our previous paper).[46] As analyzed by the SRM theory shown in Figure 1a, the terminal relaxation

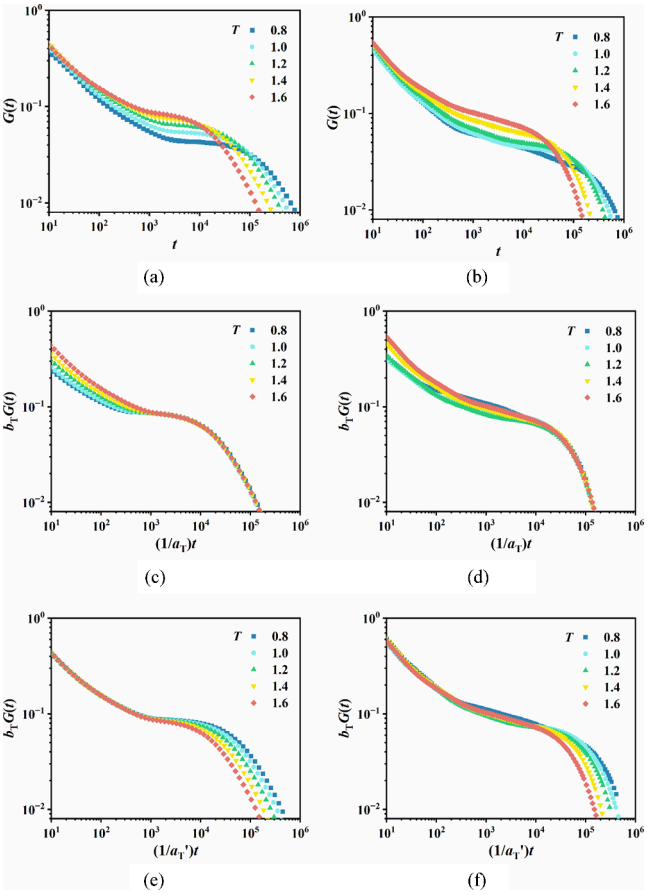

Figure 1. Left column (a), (c), (e) and right column (b), (d), (f) correspond to the results calculated using the SRM theory and molecular simulations for vitrimers, respectively. (a) and (b) show the stress relaxation modulus $G(t)$ ($E_a^k = 10$) at different temperatures. (c) and (d) display the shift factors in low-frequency superpositions. (e) and (f) present the shift factors in high-frequency superpositions.

shortens and the plateau modulus rises with the increasing temperature, with a more pronounced effect observed on the former. Using the time−temperature superposition (TTS) principle, the $G(t)$ curves are shifted with respect to a reference temperature $T_r = 1.6$. The shift factor for longer time scales (lower frequencies) is denoted as a_T (Figure 1c), while for shorter time scales (higher frequencies) is a_T' (Figure 1e). The vertical shift factor b_T is related to the ratio of the plateau modulus at a given temperature to the plateau modulus at a reference temperature T_{ref}: $b_T = G_N^0(T)/G_N^0(T_{ref})$. The failure of TTS in either the low-frequency or high-frequency region indicates that the temperature dependence of the terminal relaxation time differs between the two regions. This observation underscores the complex nature of relaxation mechanisms in APs and the necessity of a detailed understanding of their temperature-dependent behavior.[47]

It is well-known that low-frequency relaxation is associated with the terminal relaxation of the network, while high-frequency relaxation corresponds to Rouse relaxation, following Arrhenius-type and WLF-type temperature dependencies, respectively. According to the Arrhenius and WLF equations, a_T and a_T' can be written as

$$\ln(a_T) = \ln(\tau_T/\tau_{T_r}) = \frac{E_a^v}{k_B}\left(\frac{1}{T} - \frac{1}{T_r}\right) \tag{7}$$

$$\lg a_T' = \frac{-C_1(T - T_r)}{C_2 + (T - T_r)} \tag{8}$$

where E_a^v is viscous flow activation energy. C_1 and C_2 are the constants that need to be determined experimentally for each polymer system. At temperatures far above glass transition temperature T_g ($T \gg T_\infty \equiv T_r - C_2$), eq 8 can be approximated as Arrhenius relationship:

$$\ln(a_T') \approx \frac{E_a^{str}}{k_B}\left(\frac{1}{T} - \frac{1}{T_r}\right) \tag{9}$$

where

$$\frac{E_a^{str}}{k_B}\left(\frac{1}{T} - \frac{1}{T_r}\right) = \frac{-2.303C_1(T - T_r)}{C_2 + (T - T_r)} \tag{10}$$

where $\ln(a_T') = 2.303 \lg (a_T')$. This is equivalent to approximating the WLF equation as a straight line at high temperatures. E_a^{str} represents strand mobility and indicates activation energy of Rouse relaxation, while E_a^v corresponds to

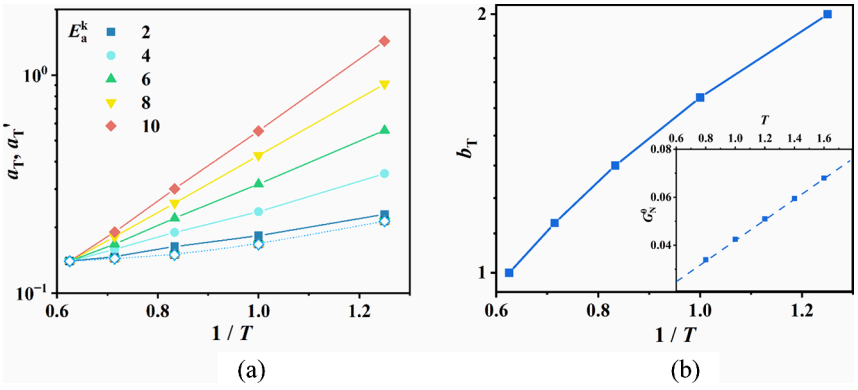

Figure 2. SRM predictions under different reaction kinetic activation energies E_a^k: (a) horizontal shift factors of a_T (solid symbols) and a_T' (hollow symbols), a_T' mainly depends on E_a^{str}, so variations in E_a^k do not alter the temperature dependence of a_T'; (b) vertical shift factors b_T. Inset: linear relationship between temperature T and plateau modulus G_N^0, with the b_T derived from G_N^0. Measured data points are connected by straight lines to illustrate the trend.

https://doi.org/10.1021/acs.macromol.4c02349
Macromolecules 2025, 58, 1898−1911

Table 1. Comparison of Three Different Energies E_a^v, E_a^{str} and E_a^k Calculated Simultaneously by SRM (with δ benchmarked) and MC/MD Hybrid Simulations at T = 1, with TTS Applied

from SRM prediction				from simulations			
input	output			input	output		
δ	E_a^{str}	E_a^v	$E_a^v - E_a^{str}$	E_a^k	E_a^{str}	E_a^v	$E_a^v - E_a^{str}$
113	1.0002	2.3087	1.3085	2	1.0001	2.3204	1.3203
132	1.0002	4.2595	3.2593	4	1.0001	4.3416	3.3415
254	1.0002	6.4195	5.4193	6	1.0001	6.2272	5.2271
889	1.0002	8.6952	7.6950	8	1.0001	8.3869	7.3868
2754	1.0002	10.7998	9.7996	10	1.0001	10.6714	9.6713

terminal relaxation. In other words, E_a^v is the total activation energy that includes E_a^{str}, with the remaining activation energy attributed to associative interactions. Here, a_T'' is defined as the ratio of a_T to a_T', and its slope represents $E_a^v - E_a^{str}$.

$$\ln(a_T'') = \ln\left(\frac{a_T}{a_T'}\right) \approx \frac{E_a^v - E_a^{str}}{k_B}\left(\frac{1}{T} - \frac{1}{T_r}\right) \tag{11}$$

For comparison, molecular simulations of APs are conducted under the same conditions as the SRM, using vitrimers to avoid the influence of sticker dissociation (which could lead to loss of cross-links). The shear stress relaxation modulus $G(t)$ is calculated from the time correlation functions of the off-diagonal components of the stress tensor $\sigma_{\alpha\beta}$ based on the Green−Kubo relationship:

$$G(t) = \frac{V}{k_B T}(\langle \sigma_{\alpha\beta}(t)\sigma_{\alpha\beta}(0)\rangle) \tag{12}$$

where V is the volume of simulated network. The multitau correlator algorithm[67] is employed to reduce the strong high-frequency noise in the simulation data and ensure efficient and accurate computation of the stress time correlation function, as shown in Figure 1b, where multiexponential fitting is applied to reveal multiple relaxation processes.

It is found that, both before and after applying the TTS principle, the simulation data (Figures 1b, 1d, 1f) agree well with the theoretical predictions (Figures 1a, 1c, 1e). The values of E_a^v and E_a^{str} from the SRM theory prediction and simulation are calculated using shift factors at different reaction kinetic activation energies E_a^k (related to δ) as shown in Figure 2 and Table 1, along with E_a^k from simulations (E_a^{str} is fitted using data at $T > 1.2$). We found that the values of $E_a^v - E_a^{str}$ obtained from SRM theory and simulation are very close and approximately equal to E_a^k, indicating that the two value of E_a^k are approximately equal, since both molecular simulation and SRM effectively capture the association interactions. Importantly, compared to pairwise interactions, the presence of four-body interactions between bonded stickers significantly reduces the probability of these stickers meeting. Therefore, the shift factors are divided by $p_{sc} \approx 0.15$ (obtained from thermodynamics analysis in our previous paper[46]) when calculating activation energies. More details refer to Section S1 of SI. Although some deviations are observed, this relationship can be approximately considered valid:

$$E_a^v \approx E_a^{str} + E_a^k \tag{13}$$

This is a significant conclusion proposed by Ricarte.[66] In fact, eq 13 is another manifestation of eq 6, demonstrating well-separated relaxation modes for full gelation, which provides evidence that the relaxation of APs is a superposition of strand motion and associative interactions. From the standpoint of decoupling, this also means that these two relaxation behaviors can be separated through shift factors in the low-frequency and the high-frequency regions.

So far, given the verification of eq 13 through simulations, it appears that we have reached the same results as Ricarte's work.[66] However, after conducting further simulations, we have gained a much deeper understanding of the LVE of APs, especially regarding activation energy and terminal relaxation time. The validation of eq 13 is actually conditional, and the decoupling of relaxation into strand motion and associative interactions may be overly simplistic. Before further discussion, we would like to introduce some of our specific simulation results, which challenge both the above conclusions and the mean-field assumption of the SRM.

3.2. Prevalence of Diffusion versus Association Interaction. In the SRM, two relaxation processes are present, shown in eq 6. Due to the decoupling of the Rouse relaxation (with the fast time scale of τ_R) and associative interaction (with the slower sticky Rouse time scale of τ_s), the terminal relaxation is predominantly governed by the slower relaxation process. This slow relaxation can be approximated as a single Maxwell relaxation mode. It is often observed that a phenomenological stretched exponential fit (KWW form)[68] is used to describe complex relaxation processes with a broad distribution of relaxation times:

$$G(t) = \frac{\nu k_B T}{N}\exp\left[\left(-\frac{t}{\tau_s}\right)^{\beta}\right] \tag{14}$$

where β is the stretching parameter, representing the distribution of relaxation times and also reflecting the complexity of the relaxation processes. τ_s represents a characteristic relaxation time, effectively averaging over the relaxation spectra and approximating the terminal relaxation time. As shown in Figure 3, single exponential fitting and the KWW fitting are compared for terminal relaxation time of the simulated vitrimers from Figure 1b. Despite both fittings yielding the same terminal relaxation time, the KWW fitting exhibits a much lower standard deviation σ_{std} = 0.00134. Similarly, discrepancies are observed between SRM predictions and MD simulation results, as shown in Figure 1 and Table 1.

We primarily attribute this to the additional relaxation modes in the simulations (discussed later), which deviate from the single-chain mean-field assumption and cause SRM to fail. Consequently, it becomes challenging to decouple the strand motion and chemical reactions and derive a complete relaxation time spectrum. This results in the dynamics of local beads not being captured by the simple decoupling of fast Rouse modes and slow sticky Rouse modes. As a result, the

https://doi.org/10.1021/acs.macromol.4c02349
Macromolecules 2025, 58, 1898−1911

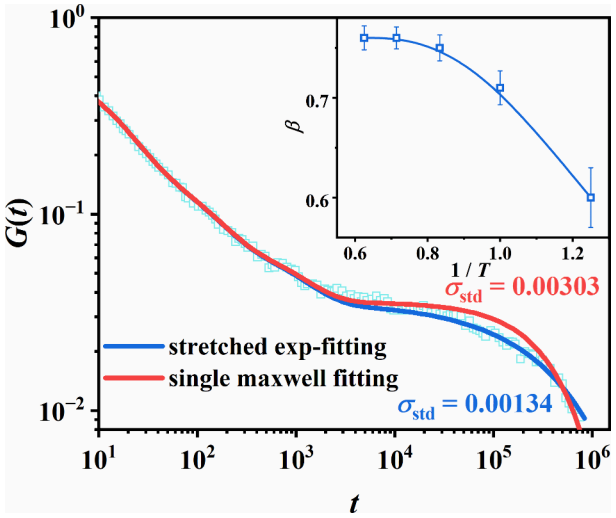

Figure 3. Stretched exponential (KWW) fittings and standard single Maxwell exponential fittings of stress relaxation modulus $G(t)$ for vitrimers with temperature T = 1.0 and E_a^k = 10, as shown in Figure 1b. Inset: stretching parameter β as a function of inverse T. The scatter plot shows the data points, while the B-spline curve illustrates the overall trends.

increased dynamic heterogeneity among beads, indicative of mixed dynamic networks, leads to broader and more complex hierarchical relaxation processes. Consequently, the KWW fitting offers a more accurate representation of this relaxation distribution, with further details provided in Section S4. This phenomenon is commonly observed in regular APs, where sticker dissociation introduces additional dynamic processes that contribute to the formation of mixed dynamic networks (namely blends of networks with varying cross-linking densities), thus reducing the plateau modulus to some extent. However, this scenario often can be ignored in the study of vitrimers.

As illustrated in the inset plot of Figure 3, β is found to be temperature-dependent, increasing with rising temperature and stabilizing at $T > 1.2$ with $\beta \approx 0.77$. The physical nature of β can be interpreted as a measure of heterogeneity, reflecting the variance in movements among individual beads. The dynamic heterogeneity of microscopic beads causes complex relaxation spectra to deviate from the single-chain SRM prediction. As β decreases and deviates further from 1, the relaxation spectra distribution broadens due to mixed dynamic networks, indicating increased dynamic heterogeneity among stickers.

Near the topology freezing transition temperature T_v (or, for regular APs, the temperature at which association begins), stickers start to unfreeze from the cross-linked network, leading to pronounced differences in mobility between the mobile and restrained beads. As the temperature increases, uniformity improves as fewer stickers remain frozen, causing β to increase and eventually reach a maximum. It is speculated that when the temperature drops further below T_g ($T_g \approx 0.53$ is measured by the specific volume change, and more details are provided in Section S3), both strand Rouse relaxation and chemical reactions (or associative interactions in regular APs) are highly suppressed. In this scenario, β will reach a minimum and become temperature-independent. Further details refer to Section S4.

From the perspective of activation energy, the change in β reflects the competition between diffusion and association interaction. It is widely acknowledged that the activation energy of the Arrhenius-type chemical reaction E_a^k does not change with temperature, meaning the relationship between the logarithm of reaction rate and inverse temperature is linear. However, diffusion behaves differently. According to Brownian dynamics, the diffusion coefficient $D = k_BT/N\xi$ is related to both temperature T and the friction coefficient ξ, where N is the chain length. As T increases, the free volume between molecular chains also increases, causing ξ to decrease. This is reflected in the Rouse model as the WLF relationship between relaxation time and inverse temperature. Extracted from the approximation in eq 9, the activation energy of segmental motion E_a^{str} increases sharply near T_g.

The relative magnitude of E_a^k to E_a^{str} are crucial for network relaxation. At low temperature close to T_g, segmental motion becomes difficult and diffusion is more challenging than reaction, implying $E_a^{str} > E_a^k$. In this diffusion-controlled state, diffusion is the key step limiting network relaxation. Conversely, at high temperature, reaction becomes more challenging since $E_a^{str} < E_a^k$, making the reaction the limiting step, known as the reaction-controlled (or association-controlled) state. Identifying the diffusion-controlled or reaction-controlled state is essential for accurately interpreting the relaxation behavior of the network. In the diffusion-controlled state, strand motion remains a non-negligible factor in the dynamics.

3.3. Loss of Cross-Links. The inevitable loss of cross-links is a common occurrence in regular APs, particularly under weak associative interaction (low E_a^k). In contrast, the cross-linking density of vitrimers remains constant due to BERs, distinguishing them from regular APs. This disparity in viscoelastic behavior has been thoroughly discussed in our earlier work,[46] both linearly and nonlinearly. Here, we aim to understand its contribution to terminal relaxation from the perspective of molecular motion.

Returning to the homogeneous simulation of APs with 4 stickers equally distributed on a polymer chain of 50 beads, the mean square displacement (MSD) of all stickers, $\triangle r^2(t)$, is calculated under E_a^k = 2∼10 and T = 0.4∼1.6, as presented in Figure 4. Notably, as described in eq 6, when the terminal relaxation is successfully decoupled into fast Rouse modes and slow sticky Rouse modes, the diffusion of the network on long time scales is primarily dominated by the slow relaxation due to associative friction. Stickers exhibit diffusion behavior similar to the center-of-mass motion averaged over all chains (Figure S7 in the SI), further confirming that the diffusion of stickers reliably approximates the long-time diffusion dynamics, additional details are provided in Section S5.

Besides, the interpretation of reaction kinetic activation energies E_a^k differs between the two networks. In vitrimers, E_a^k represents the activation energy for exchange reactions, while in regular APs, it generally includes both dissociation and association activation energies. Since association typically does not require energy (or may even have a negative value), E_a^k primarily refers to the dissociation activation energy in this context. Figures 4a and 4c analyze the MSD dependence on various E_a^k at T = 1, while Figures 4b and 4d examine the MSD dependence on T at a moderate activation energy E_a^k = 6. This range of E_a^k spans from weak to strong association, covering T from T_g to T_v for vitrimers ($T_v \approx 0.82$, the definition and values of T_v are discussed in Figure 5 below).

As E_a^k increases, the dissociative interaction slows down, resulting in decreased diffusion of the stickers, as their diffusion

https://doi.org/10.1021/acs.macromol.4c02349
Macromolecules 2025, 58, 1898−1911

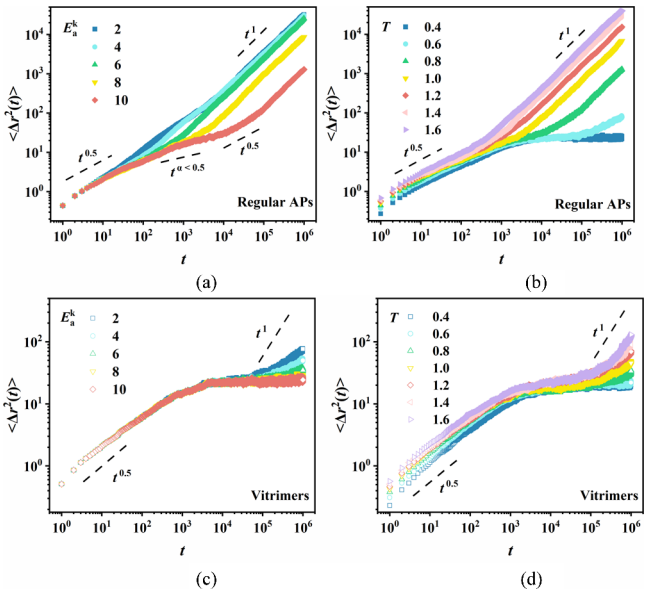

Figure 4. Mean squared displacements $\langle r^2(t)\rangle$ vs time t of all sticker are shown for regular APs and vitrimers. Panels (a) and (c) present the results for varying reaction kinetic activation energies at temperature T = 1, and panels (b) and (d) illustrate the effect of temperature at E_a^k = 6.

is influenced by both strand motion and chemical reactions. Four distinct regions are observed in the MSD curves as time t increases: the first Rouse region, the plateau region, the second Rouse region and the Fickian diffusion region. Furthermore, due to the slow four-body interactions in the vitrimer, a longer time scale is required to reach the final Fickian diffusion region. The increase in temperature enhances the motion of stickers across all four regions, whereas E_a^k affects only the last three regions since association can occur only on time scales longer than the Rouse time scale. Notably, the diffusion of vitrimers (Figures 4c, 4d) is slower by 2 orders of magnitude compared to regular APs (Figures 4a, 4b), which can be attributed to the four-body interactions inherent in our simulation algorithm that maintains cross-links density. Despite this difference, regular APs and vitrimers exhibit similar behaviors. This observation highlights the necessity of understanding the underlying molecular motions contributing to terminal relaxation in both systems.

However, distinctions become apparent after applying the TTS principle, as shown in Figures 5a, 5b. The applicability of the TTS principle to MSD is grounded in the generalized Stokes−Einstein relationship:[36]

$$G(s) = \frac{k_B T}{\pi R \langle \triangle r^2(s) \rangle} \tag{15}$$

where $G(s)$ represents the Laplace transformation of the relaxation modulus $G(t)$ in frequency space s, and $\triangle r^2(s)$ is the Laplace transform of the MSD $\triangle r^2(t)$ of Brownian tracers with radius R, which are considered as reactive units in this context. eq 15 illustrates that $G(t)$ and $\triangle r^2(t)$ can be converted into each other as they share the same scale of motion units. The MSD curves are shifted to a longer time scale with the reference temperature T_r = 1.0. The resulting pseudo-TTS master curves reveal distinct temperature dependencies.

The horizontal shift factor as a function of inverse temperature is depicted in Figure 5c. For vitrimers, there is a clear transition from WLF dependence ($T \leq 0.8$) to Arrhenius dependence ($T > 0.8$). This transition temperature, known as the topological freezing transition temperature T_v, marks the point where the chemical reactions start or significantly accelerate. In contrast, the transition region for regular APs is quite broad. Arrhenius fitting does not seem suitable at high temperatures, which can be attributed to sticker dissociation. As the temperature increases, the reversible associative interaction tends to shift toward dissociation, gradually decreasing the cross-linking density and disrupting the dynamic network. In the absence of a cross-links, the motion of stickers becomes unrestrained, resulting in faster relaxation at higher temperatures.

In our previous work,[46] we compared the $G(t)$ of Diss-CANs (regular APs) with that of Asso-CANs (vitrimers), revealing that the distinction between these two networks lies in the prefactor of the terminal relaxation time τ_s^0,

$$\tau_s = \tau_s^0 \exp(E_a^v / k_B T) \tag{16}$$

This is consistent with the temperature dependence of the shift factor observed in this paper. On the one hand, it indicates that, besides strand motion and associative interactions, there is another mechanism for relaxing the cross-linked network, such as sticker dissociation. As the temperature increases and E_a^k decreases, this special relaxation

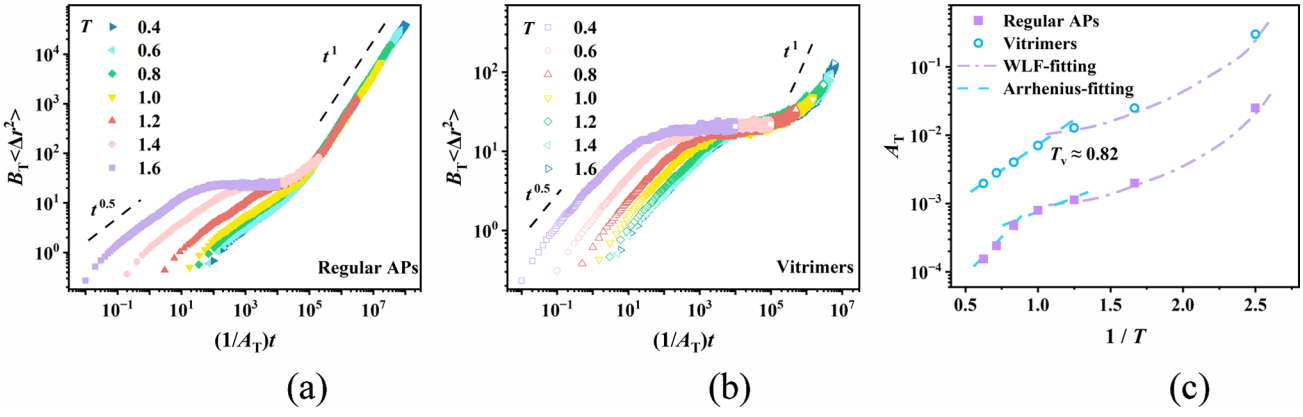

Figure 5. Shifting MSD curves of (a) regular APs and (b) vitrimers to long time scale based on the TTS principle. (c) Temperature dependence of shift factors, with purple and blue dashed lines representing WLF-fitting and Arrhenius fitting, respectively.

https://doi.org/10.1021/acs.macromol.4c02349
Macromolecules 2025, 58, 1898−1911

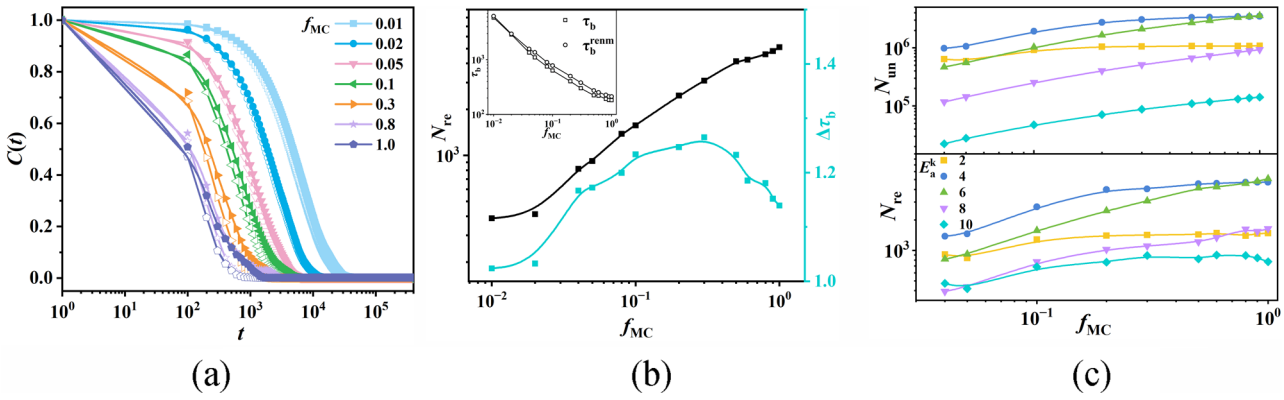

Figure 6. Under different f_{MC} values with $E_a^k = 6$ and $T = 1$: (a) bond autocorrelation functions $C(t)$ of RAN (solid symbols) and RFN (hollow symbols); (b) the f_{MC} dependence of $\Delta\tau_b$ and N_{re}, with a subplot showing bond lifetimes of RAN and RFN. (c) The f_{MC} dependence of N_{un} and N_{re} across various E_a^k. Data points are shown with B-spline curve fitting to illustrate trends.

behavior becomes increasingly prominent for regular APs. Under extreme conditions, the network may practically cease to exist. On the other hand, the influence of this relaxation is independent of activation energy, meaning that only the encounter probability between stickers is affected. Therefore, sticker dissociation can be effectively decoupled from associative interactions by the prefactor τ_s^0 of the terminal relaxation time τ_s.

The loss of cross-linking density due to existence of sticker dissociation directly demonstrates the violation of eq 13, which essentially challenges both the SRM and the mean-field assumption. Consequently, our simulation results should be viewed as supplements to the theoretical framework, offering a more comprehensive understanding of the relaxation mechanisms in APs.

3.4. Reassociation. Among APs, segments regain mobility following sticker dissociation, allowing for network rearrangement. Recent theoretical and experimental studies have emphasized the distinction between bond dissociation time and bond rearrangement time (where stickers change partners at this time scale, thus contributing to stress relaxation).[56−59] The distinction between these two time scales has been described by bond lifetime renormalization model.[56] Particularly, at weak dissociation energy ($E_a \ll RT \ln N$), the correlations between stickers can be neglected. In the intermediate bond-energy regime ($RT \ln N < E_a < 2RT \ln N$), stickers exhibit short lifetimes, numerous open stickers exist within the range of dangling chains. Before the random walk volume becomes large enough to encounter a new partner, open stickers tend to reassociate with their original partner. This reassociation extends the bond rearrangement time beyond the bond dissociation time, introducing a delay in terminal relaxation. At higher dissociation energies ($E_a > 2RT \ln N$), the lower concentration of open stickers renders the two time scales comparable. Remarkably, the bond dissociation energy in regular APs is approximated to the reaction kinetic activation energies E_a^k, thus we primarily regulating E_a^k during simulations.

The renormalized bond lifetime τ_b^{renm} can be defined as the average time for a sticker to bond with a new sticker after its initial bonding event.[56] τ_b^{renm} includes both the duration for the open sticker to reassociate with its original partner and the time τ_{open} required for the open sticker to associate with a new partner:

$$\tau_b^{renm} \approx J(\tau_{open})\tau_b + \tau_{open} \tag{17}$$

In this equation, $J(\tau_{open})$ (a function of τ_{open}) represents the number of reassociation events, with each event lasting for a duration of bond lifetime τ_b. Given the absence of an open sticker state in vitrimers, our primary focus was on exploring the relaxation mode caused by reassociation in regular APs. The bond lifetime of stickers τ_b can be calculated from the bond autocorrelation function $C(t)$:

$$C(t) = \frac{\langle H(t + t_0)H(t_0)\rangle}{\langle H(t_0)^2\rangle} \tag{18}$$

where $H(t)$ is a binary function, if a pair of stickers remains bonded during the time interval t, $H(t) = 1$; and $H(t) = 0$ otherwise. Using trajectories from molecular simulation, eq 18 provides information about each sticky bond. To trace the reassociation, two algorithms are designed: the reassociation-free network (RFN) and the reassociation-allowing network (RAN), corresponding to bond lifetimes τ_b and τ_b^{renm}, respectively, of which the former is more easily obtained in simulations than in experiments. These two bond lifetimes are determined by fitting $C(t)$ to the forms of $\exp(-t/\tau_b)$ and $\exp(-t/\tau_b^{renm})$. In the RFN, reassociation of stickers after dissociation is not allowed, meaning the bond state sequence $H(t)$ is monotonous and can only change from 1 to 0 (the transition point corresponds to the first bond dissociation). Conversely, two stickers can reassociate after dissociating in RAN, resulting in a randomly ordered bond state sequence of $H(t)$. The reassociation factor $\Delta\tau_b$ was introduced to quantify the degree of reassociation, defined as $\Delta\tau_b = \tau_b^{renm}/\tau_b$, with a larger $\Delta\tau_b$ indicating more prominent reassociation.

Remarkably, since reassociation behavior occurs only within the time scale before the network enters terminal relaxation, τ_s was introduced as the threshold in the algorithm to balance computational accuracy and efficiency. Time scales $t < \tau_s$ are considered effective for capturing reassociations that influence terminal relaxation, with further details provided in Section S6. Besides E_a^k, f_{MC} also plays a critical role in directly impacting reassociation. In our hybrid MC/MD algorithm, f_{MC} governs the proportion of stickers selected in each MC step, the more stickers available for reaction, the higher the probability of reassociation. We hypothesize that compared to the indirect regulation by E_a^k, f_{MC} exerts a more instant impact on bond lifetimes. Consequently, f_{MC} is initially incorporated into the prefactor of the bond lifetimes:

https://doi.org/10.1021/acs.macromol.4c02349
Macromolecules 2025, 58, 1898−1911

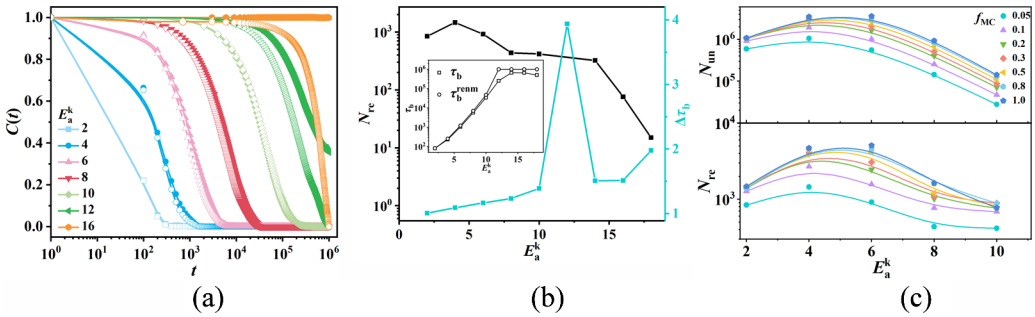

Figure 7. Under different E_a^k values with f_{MC} = 0.05and T = 1: (a) bond autocorrelation functions $C(t)$ of RAN (solid symbols) and RFN (hollow symbols); (b) the E_a^k dependence of $\Delta\tau_b$ and N_{re}, with a subplot showing bond lifetimes of RAN and RFN. (c) The E_a^k dependence of N_{un} and N_{re} across various f_{MC}. Scatter points are simulation data, connected by B-spline interpolation for clarity.

$$\tau_b^0 \propto \frac{1}{f_{MC}} \tag{19}$$

Therefore, we focus on both E_a^k and f_{MC} when investigating reassociation. Using the same simulated network as last section, $C(t)$ is calculated under the same E_a^k but with varying f_{MC}, as shown in Figures 6a and 6b. As f_{MC} increases, more selected stickers accelerate the bond exchange, leading to a faster decay of $C(t)$ and shorter bond lifetimes. Furthermore, for the same f_{MC}, the decay of RAN is consistently slower than that of RFN. Similarly, τ_b^{renm} consistently exceeds τ_b under the same f_{MC}, both confirming the occurrence of reassociation. This f_{MC} dependence of τ_b^{renm}, τ_b and$\Delta\tau_b$ is consistent across various E_a^k, as further explained in the SI. As illustrated in Figure 6c, within the E_a^k range of 2 to 10, the number of sticker reassociation N_{re} and dissociations N_{un} increase with f_{MC}, implying that the enhanced reassociation is strongly related to the number of stickers involved in associative interactions.

The influence of E_a^k on reassociation is also simulated under f_{MC} = 0.05. As depicted in Figures 7a and 7b, increasing E_a^k makes it more challenging for stickers to dissociate, resulting in longer bond lifetimes. Under the same E_a^k, the relaxation of RAN is consistently slower than that of RFN. Figure 7b shows that N_{re} and $\Delta\tau_b$ exhibit a nonmonotonic dependence on E_a^k, with more details on how τ_b^{renm}, τ_b and$\Delta\tau_b$ vary with E_a^k under different f_{MC} provided in the SI. Notably, it is surprising to find that the maximum values of both N_{re} and N_{un} across all f_{MC} occur in the same activation energy regime ($2 < E_a^k < 6$) in Figure 7c, which aligns with the intermediate activation energy regime $RT \ln N < E_a^k < 2RT \ln N$ (where the average dangling chain length N = 12.5 in our simulations). This regime matches the bond lifetime renormalization model's prediction of the strongest reassociation effects. And the trend holds true across all f_{MC} values, showing a good agreement with the theoretical model. The curves for f_{MC} = 0.8 and f_{MC} = 1.0 are quite comparable, suggesting that f_{MC} is approaching its limit for regulating reassociation. Specifically, different f_{MC} values only affect the magnitude rather than the shape of the curve, indicating that f_{MC} can be effectively separated from the reassociation effect. This corroborates the rationality of incorporating f_{MC} into the prefactor of the bond lifetime in eq 19.

Noting that $\Delta\tau_b$ is less sensitive than N_{re}. For instance, our findings reveal that $\Delta\tau_b$ exhibits a nonmonotonic dependence on E_a^k and f_{MC} in Figures 6b and 7b, which does not fully correspond with the theoretical model. Since we incorporate f_{MC} to control the number of stickers engaged in reactions, whereas the bond lifetime renormalization model does not impose a similar constraint, it is reasonable to speculate that the combined influence of f_{MC} and E_a^k on relaxation behavior leads to some deviations from the theory, with a detailed analysis presented in the SI. Overall, $\Delta\tau_b$ quantifies the degree of reassociation indirectly via relaxation time, which may show some distribution as it represents an average value. In contrast, N_{re} provides a more intuitive measure. Since there may be other relaxation modes that might affect bond lifetimes and $\Delta\tau_b$, future investigations will focus on establishing a more consistent relationship between microscale bond lifetimes and macroscopic rheological properties.

3.5. Small Molecule Reactants. In current research, the single chain model is typically employed in theoretical studies, while simulations often prefer coarse-grained molecular chains. These approaches tend to ignore the size effect of stickers participating in associative interactions. It is widely reported that small molecule reactants are often involved, such as the coordinated motion of lithium ions in PEO-based polyelectrolytes[69] and the dioxaborolane metathesis reaction in vitrimers.[52,53] When simulating self-repair materials, we found that[70] the introduction of small-sized cross-linkers can greatly accelerate the healing process, indicating a unique relaxation behavior.

As shown in Figure S3 of the SI, we designate the ends of cross-linker chains as stickers, with cross-linker chain lengths N_{cl} = 2∼8. The linear polymer chains maintain the same structure as described in Figure S2, with a length of N = 50 beads and 4 equally distributed stickers. However, in this setup, the stickers can only bond with cross-linkers, instead of with stickers on other chains. To avoid phase separation, each sticker is restricted to associate with only one cross-linker at a time. Figures 8a, 8b illustrate simulations of vitrimers and regular APs under E_a^k = 6 and 10 (results for E_a^k = 8 are added in Figure S10). To emphasize the effects of segment motion, a relatively low temperature of T = 1.0 is chosen. As E_a^k increases, the terminal relaxation times τ_s of APs with different N_{cl} gradually diverge, with shorter cross-linkers leading to faster relaxation times. Compared with the homogeneous network (hollow blue symbols), the terminal relaxation time with N_{cl} = 2 (solid blue symbols) shortens by as much as 2/3 for vitrimers and by 1/2 for regular APs.

Given the same difficulty of associative interactions represented by E_a^k, the relaxation is primarily governed by strand mobility. As the cross-linker size decreases, strand mobility is enhanced, effectively minimizing or even eliminating E_a^{str}. This effect is less pronounced in APs with low E_a^k since frequent network rearrangements already mitigate the impact of enhanced diffusion. For regular APs, the acceleration of

https://doi.org/10.1021/acs.macromol.4c02349
Macromolecules 2025, 58, 1898−1911

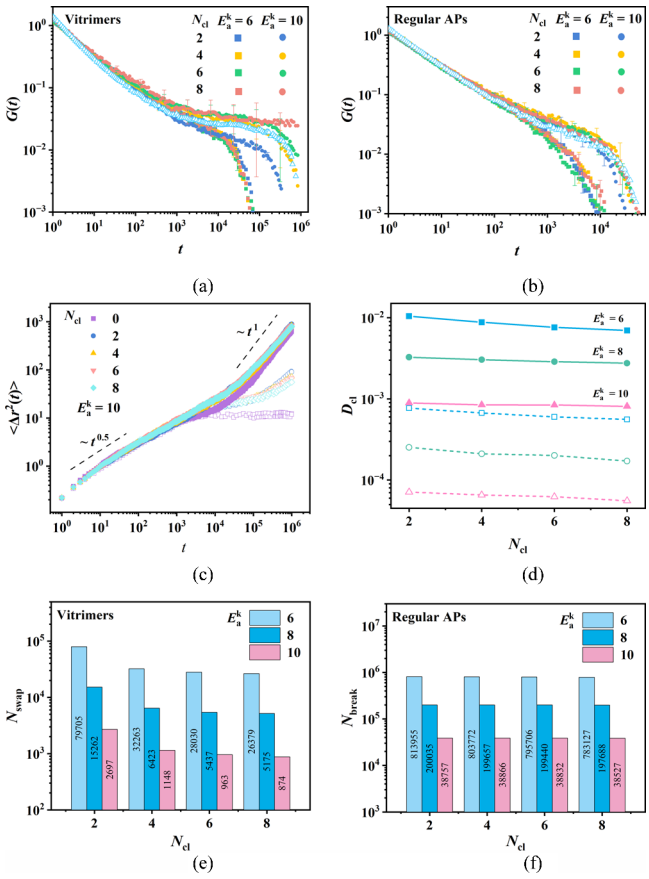

Figure 8. Cross-linker chain length N_{cl} dependence of: (a) stress relaxation modulus $G(t)$ in vitrimers and (b) regular APs, circle and square symbols correspond to E_a^k = 10,6, hollow blue symbols represent regular APs without cross-linker and with E_a^k = 10 and T = 1, chain length shorter than 4 exhibit faster relaxation; (c) MSD and (d) diffusion coefficient D_{cl} of regular APs (solid symbols) and vitrimers (hollow symbols), simulation data points are shown, with straight lines connecting them to illustrate the trend; (e) number of bond swap in vitrimers (N_{swap}) and (f) sticker dissociation in regular APs (N_{break}).

relaxation is less significant compared to vitrimers, because their terminal relaxation time is already considerably shorter. Additionally, the presence of open stickers in regular APs allows for cross-linker diffusion that is partially or completely independent of the molecular chains, leading to a more pronounced effect and faster relaxation. Consequently, we propose that small molecule reactants exert a more substantial influence on regular APs compared to vitrimers under the same conditions.

The MSD is also calculated as shown in Figure 8c. Compared to the network without cross-linkers (purple symbols), the introduction of cross-linkers of varying sizes all enhances diffusion, with shorter cross-linkers exhibiting a higher diffusion coefficient (Figure 8d), consistent with the relation $D = k_BT/N\xi$. From this perspective, the reduction of E_a^{str} arises because polymer (strand) relaxation is effectively replaced by the diffusion of small molecule cross-linkers. Besides, the number of successful bond swaps in vitrimers (N_{swap}) and sticker dissociations in regular APs (N_{break}) are computed, as shown in Figures 8e, 8f. Although the probability remains unchanged (dependent only on temperature and activation energy), the overall quantities significantly increase as N_{cl} decreases. By combining $\langle t \rangle$, D, and N_{swap}, we found that cross-linkers promote vitrimer relaxation more effectively than regular APs, with vitrimers showing a stronger dependence on cross-linker size. This is not only because strand relaxation in vitrimers is replaced by the diffusion of small molecule cross-linkers, but also due to the presence of open stickers in regular APs.

For APs with strong reaction kinetic activation energy, only a few small molecule reactants are needed to significantly accelerate the network rearrangement. In such cases, the relaxation process remains primarily governed by the polymer chains with the activation energy E_a^{str} for strand motion. By carefully designing reactions, when strand relaxation is replaced by small molecules, eq 13 may simplify to $E_a^v \approx E_a^k$ in extreme cases, which serves as further validation of decoupling. For example, in Figure 8f, although the dependence of N_{break} on cross-linker size is not significant, a more pronounced dependence on E_a^k is observed, further demonstrating that decoupling of E_a^k and E_a^{str} can still be achieved in this case. In other words, eq 13 represents a significant outcome under the mean-field assumption, enabling the adoption of the SRM. The replacement of strand relaxation by small molecules can be particularly beneficial for applications of APs requiring fast relaxation, such as in fast self-healing materials.

3.6. Discussions. Based on our simulation results, we have identified additional relaxation mechanisms in APs beyond strand motion and associative interactions that are rarely discussed. Taking all these factors into account, we propose the following universal expression for the terminal relaxation time τ_s:

$$\tau_s \sim J(\alpha_{str} p_{cl} \tau_{rea} + \tau_{str}) \tag{20}$$

where p_{cl} presents the existing ratio of cross-links, J denotes the average number of reassociation, and τ_{str} and τ_{rea} correspond to the relaxation times due to strand motion and associative interactions driving network rearrangement, respectively. The parameter α_{str} quantifies the dependency of chemical reactions on strand motion. A large α_{str} indicates a strong dependence on strand motion, leading to longer relaxation times due to chemical reactions. Conversely, a small α_{str} signifies minimal dependence, resulting in significantly shorter relaxation times. This expression accounts for strand motion, associative interactions, cross-linking density, and reassociation effects on relaxation behavior. By expressing τ_s in exponential form and taking the logarithm of both sides, we can separate the prefactor and activation energy contributions:

$$\ln \tau_s = \ln \tau_s^0 + \frac{E_a^v}{k_BT} \approx \ln J + \frac{E_a^{str}}{k_BT} + \ln(p_{cl}\tau_{rea}^0) + \frac{E_a^k}{k_BT} \tag{21}$$

The prefactor $\tau_s^0 \sim p_{cl}\tau_{rea}^0$ highlights that relaxation due to cross-link loss is reflected in the prefactor, consistent with observations in both experiments by Chen et al.[71] and our simulations.[46] Moreover, the effect of f_{MC} on reassociation can be incorporated into the prefactor of bond lifetime τ_b^0. Although its contribution to terminal relaxation is less pronounced than that of the activation energy, it should not be ignored.

The validity of eq 21 can be verified in certain limiting cases. First, when p_{cl} = 0 (indicating that all stickers have dissociated), the terminal relaxation of such network in eq 20 depends on the relaxation of nonsticky chains. Additionally,

https://doi.org/10.1021/acs.macromol.4c02349
Macromolecules 2025, 58, 1898−1911

for vitrimers with strong activation energy (where $p_{cl} = 1$ and reassociation can be ignored), eq 21 can be simplified to eq 13 ($E_a^v \approx E_a^{str} + E_a^k$), which has been validated not only through the SRM and simulations in Section 3.1, but also by experimental studies.[17]

The significance of eq 21 lies in the decoupling of each relaxation behaviors and the definition of their influence; consequently, the temperature dependence of the shift factor (or terminal relaxation time) can be depicted in Figure 9. The

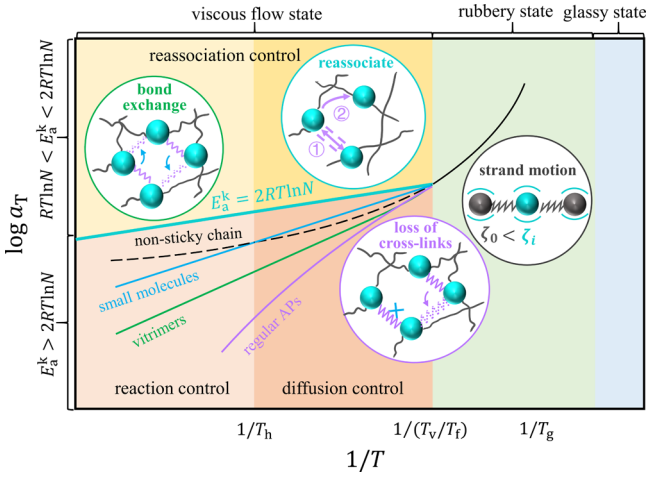

Figure 9. Schematic diagram illustrating the temperature dependence of the shift factor (or terminal relaxation time) for APs exhibiting different relaxation modes

phase diagram is divided into several regions by reaction kinetic activation energy and temperature, with each region distinguished by different colors. Below the glass transition temperature T_g, the segmental motion is frozen in the glassy state, which inhibits the network from relaxing and leads to an effectively infinite terminal relaxation time. With the temperature rises above T_g and the network transitions into the rubbery state, the strands between stickers gain sufficient free volume to move, where the relaxation follows the WLF equation. As the temperature further increases to the point where the associative interactions become possible, several new relaxation modes begin to emerge.

Vitrimers, which possess bond exchange reactions while maintaining a constant cross-linking density, exhibit Arrhenius-type relaxation, appearing as a straight line (green line) at high temperatures. In contrast, regular APs undergo a process of association and dissociation, accompanied by the loss of cross-links. This behavior is reflected in the phase diagram as accelerated relaxation compared to vitrimers (purple line). Both networks demonstrate a coupled relaxation with strand motion, leading to a diffusion-controlled region at temperatures slightly above T_v or T_f. Here, T_f, referring to the flow temperature primarily used to describe the dissociation and association behavior in regular APs, is further explained in Section S3 of the SI. In this region, the influence of segmental movement primarily manifests in the distribution of terminal relaxation times, except when $T_v/T_f \gg T_g$, where the relaxation time itself is also affected since WLF-type relaxation is faster than Arrhenius-type relaxation. As the temperature continues to rise, the dependence of segmental mobility weakens and this region transitions into the reaction-controlled region, with the critical temperature defined as T_h. However, vitrimers with small molecule reactants are not constrained by strand motion, and their viscous flow activation energy is close to their reaction kinetic activation energy, resulting in a straight line with a lower slope (blue line).

The discussion above assumes the condition of $E_a^k > 2RT \ln N$, namely strong reaction kinetic activation energy, where reassociation occurs relatively infrequently. When $RT \ln N < E_a^k < 2RT \ln N$, the phase diagram introduces a separate region (cyan line), where reassociation may become dominant. In this region, other relaxation modes also exist, making it challenging to provide a straightforward description. Consequently, the terminal relaxation time under $RT \ln N < E_a^k < 2RT \ln N$ is not shown in the phase diagram. However, Figure 9 strongly suggests that the effect of reassociation must be considered when discussing the relaxation under intermediate reaction kinetic activation energy, as verified by both simulation and theory. Further exploration will focus on decoupling reassociation from other relaxation modes to achieve a more precise mathematical expression. As research into various relaxation modes deepens, our comprehension of the LVE of APs is certain to become increasingly sophisticated.

4. CONCLUSIONS

We aim to reinterpret the LVE of APs by exploring it through the lens of decoupling. Instead of attributing relaxation behavior solely to the combination of strand motion and associative interactions, we propose that the overall relaxation behavior is determined by multirelaxation modes, including strand motion, association reaction, loss of cross-links density and reassociation, while exhibiting a distribution.

Derived from the SRM, the relationship $E_a^v \approx E_a^{str} + E_a^k$ indicates that the segmental motion and associative interactions can be separated in a fully gelated network, which is supported by our simulation works. However, we find this relationship invalid under certain conditions. Initially, for regular APs with weak reaction kinetic activation energy, sticker dissociation introduces additional relaxation such as the loss of cross-links, which can be decoupled from associative interactions by the prefactor of the terminal relaxation time. Subsequently, under moderate reaction kinetic activation energy, reassociation plays an important role and strongly affects terminal relaxation behavior. Furthermore, the disparity between the activation energy required for strand motion and the magnitude of reaction kinetic activation energy between stickers determines the distribution of the terminal relaxation time. Ultimately, when small molecule reactants are involved, the relaxation of strands is replaced by cross-linkers, with terminal relaxation primarily driven by associative interactions. By decoupling various relaxation modes in the overall terminal relaxation of APs, we aim to achieve an accurate analysis of their viscoelastic behavior at the microscopic level.

■ ASSOCIATED CONTENT

Supporting Information

The Supporting Information is available free of charge at https://pubs.acs.org/doi/10.1021/acs.macromol.4c02349.

S1. Hybrid MC/MD algorithm of regular APs and vitrimers. **S2.** Benchmarking the hybrid MC/MD algorithm. **S3.** Glass transition temperature (T_g) and topological freezing transition temperature (T_V). **S4.** KWW fitting. **S5.** The mean squared displacements (averaged over all chains at the center-of-mass). **S6.**

https://doi.org/10.1021/acs.macromol.4c02349
Macromolecules 2025, 58, 1898−1911

Terminal relaxation time. **S7.** The bond lifetime and reassociation factor $\Delta\tau_b$ under different values of f_{MC} and E_a^k. **S8.** The cross-linker chain length N_{cl} dependence on $G(t)$ (PDF)

AUTHOR INFORMATION

Corresponding Author

Ping Tang − *State Key Laboratory of Molecular Engineering of Polymers, Department of Macromolecular Science, Fudan University, Shanghai 200433, China;* orcid.org/0000-0003-0253-1836; Email: pingtang@fudan.edu.cn

Authors

Xiang Cui − *State Key Laboratory of Molecular Engineering of Polymers, Department of Macromolecular Science, Fudan University, Shanghai 200433, China*

Yulin Luo − *State Key Laboratory of Molecular Engineering of Polymers, Department of Macromolecular Science, Fudan University, Shanghai 200433, China*

Yuliang Yang − *State Key Laboratory of Molecular Engineering of Polymers, Department of Macromolecular Science, Fudan University, Shanghai 200433, China*

Complete contact information is available at: https://pubs.acs.org/10.1021/acs.macromol.4c02349

Author Contributions

[+]X.C. and Y.L. contributed equally.

Notes

The authors declare no competing financial interest.

ACKNOWLEDGMENTS

The authors thank the financial support from the National Natural Science Foundation of China (grant nos. 22373023 and 21973017).

REFERENCES

(1) Jin, Y.; Yu, C.; Denman, R. J.; Zhang, W. Recent advances in dynamic covalent chemistry. *Chem. Soc. Rev.* **2013**, *42* (16), 6634−6654.

(2) Davis, V. A.; Ericson, L. M.; Parra-Vasquez, A. N. G.; Fan, H.; Wang, Y.; Prieto, V.; Longoria, J. A.; Ramesh, S.; Saini, R. K.; Kittrell, C.; et al. Phase Behavior and Rheology of SWNTs in Superacids. *Macromolecules* **2004**, *37* (1), 154−160.

(3) Brizzolara, D.; Cantow, H.-J.; Diederichs, K.; Keller, E.; Domb, A. J. Mechanism of the Stereocomplex Formation between Enantiomeric Poly(lactide)s. *Macromolecules* **1996**, *29* (1), 191−197.

(4) Borukhov, I.; Leibler, L. Enthalpic Stabilization of Brush-Coated Particles in a Polymer Melt. *Macromolecules* **2002**, *35* (13), 5171−5182.

(5) Zhang, S.; Qin, Y.; Uddin, M. A.; Jang, B.; Zhao, W.; Liu, D.; Woo, H. Y.; Hou, J. A Fluorinated Polythiophene Derivative with Stabilized Backbone Conformation for Highly Efficient Fullerene and Non-Fullerene Polymer Solar Cells. *Macromolecules* **2016**, *49* (8), 2993−3000.

(6) Fox, J. D.; Rowan, S. J. Supramolecular Polymerizations and Main-Chain Supramolecular Polymers. *Macromolecules* **2009**, *42* (18), 6823−6835.

(7) Yamauchi, K.; Lizotte, J. R.; Long, T. E. Thermoreversible Poly(alkyl acrylates) Consisting of Self-Complementary Multiple Hydrogen Bonding. *Macromolecules* **2003**, *36* (4), 1083−1088.

(8) Chen, Q.; Huang, C.; Weiss, R. A.; Colby, R. H. Viscoelasticity of Reversible Gelation for Ionomers. *Macromolecules* **2015**, *48* (4), 1221−1230.

(9) Weiss, R. A.; Yu, W.-C. Viscoelastic Behavior of Very Lightly Sulfonated Polystyrene Ionomers. *Macromolecules* **2007**, *40* (10), 3640−3643.

(10) Chen, Q.; Tudryn, G. J.; Colby, R. H. Ionomer dynamics and the sticky Rouse modela. *J. Rheol.* **2013**, *57* (5), 1441−1462.

(11) Huang, C.; Chen, Q.; Weiss, R. A. Rheological Behavior of Partially Neutralized Oligomeric Sulfonated Polystyrene Ionomers. *Macromolecules* **2017**, *50* (1), 424−431.

(12) Liu, S.; Zhang, Z.; Chen, Q.; Matsumiya, Y.; Watanabe, H. Nonlinear Rheology of Telechelic Ionomers Based on Sodium Sulfonate and Carboxylate. *Macromolecules* **2021**, *54* (20), 9724−9738.

(13) Wang, W.; Madsen, J.; Genina, N.; Hassager, O.; Skov, A. L.; Huang, Q. Toward a Design for Flowable and Extensible Ionomers: An Example of Diamine-Neutralized Entangled Poly(styrene-co-4-vinylbenzoic acid) Ionomer Melts. *Macromolecules* **2021**, *54* (5), 2306−2315.

(14) Montarnal, D.; Capelot, M.; Tournilhac, F.; Leibler, L. Silica-Like Malleable Materials from Permanent Organic Networks. *Science* **2011**, *334* (6058), 965−968.

(15) Zhang, W.; Zhang, H.; Yang, Y.; Tang, P. Poly(maleic acid-co-acrylic acid) ionomer as nucleating agent on the crystallization behavior and properties of poly(ethylene terephthalate). *Polym. Bull.* **2022**, *79* (6), 3803−3827.

(16) Zhang, W.; Zhang, H.; Yang, L.; Tang, Y.; Tang, P. Enhanced crystallization and properties of poly(ethylene terephthalate) nanocomposites with zeolites from 3D to 2D topologies. *Journal of Industrial and Engineering Chemistry* **2022**, *109*, 510−520.

(17) Zhang, W.; Cui, X.; Zhang, H.; Yang, Y.; Tang, P. Linear viscoelasticity, nonlinear rheology and applications of polyethylene terephthalate vitrimers. *J. Polym. Sci.* **2023**, 2010.

(18) Zhang, C.; Yang, Z.; Duong, N. T.; Li, X.; Nishiyama, Y.; Wu, Q.; Zhang, R.; Sun, P. Using Dynamic Bonds to Enhance the Mechanical Performance: From Microscopic Molecular Interactions to Macroscopic Properties. *Macromolecules* **2019**, *52* (13), 5014−5025.

(19) Porath, L.; Huang, J.; Ramlawi, N.; Derkaloustian, M.; Ewoldt, R. H.; Evans, C. M. Relaxation of Vitrimers with Kinetically Distinct Mixed Dynamic Bonds. *Macromolecules* **2022**, *55* (11), 4450−4458.

(20) Ge, S.; Tsao, Y.-H.; Evans, C. M. Polymer architecture dictates multiple relaxation processes in soft networks with two orthogonal dynamic bonds. *Nat. Commun.* **2023**, *14* (1), 7244.

(21) Suzuki, S.; Uneyama, T.; Inoue, T.; Watanabe, H. Nonlinear Rheology of Telechelic Associative Polymer Networks: Shear Thickening and Thinning Behavior of Hydrophobically Modified Ethoxylated Urethane (HEUR) in Aqueous Solution. *Macromolecules* **2012**, *45* (2), 888−898.

(22) Uneyama, T.; Suzuki, S.; Watanabe, H. Concentration dependence of rheological properties of telechelic associative polymer solutions. *Phys. Rev. E* **2012**, *86* (3), No. 031802.

(23) Suzuki, S.; Uneyama, T.; Watanabe, H. Concentration Dependence of Nonlinear Rheological Properties of Hydrophobically Modified Ethoxylated Urethane Aqueous Solutions. *Macromolecules* **2013**, *46* (9), 3497−3504.

(24) Chen, Q.; Zhang, Z.; Colby, R. H. Viscoelasticity of entangled random polystyrene ionomers. *J. Rheol.* **2016**, *60* (6), 1031−1040.

(25) Wu, S.; Cao, X.; Zhang, Z.; Chen, Q.; Matsumiya, Y.; Watanabe, H. Molecular Design of Highly Stretchable Ionomers. *Macromolecules* **2018**, *51* (12), 4735−4746.

(26) Shabbir, A.; Huang, Q.; Baeza, G. P.; Vlassopoulos, D.; Chen, Q.; Colby, R. H.; Alvarez, N. J.; Hassager, O. Nonlinear shear and uniaxial extensional rheology of polyether-ester-sulfonate copolymer ionomer melts. *J. Rheol.* **2017**, *61* (6), 1279−1289.

(27) Green, M. S.; Tobolsky, A. V. A New Approach to the Theory of Relaxing Polymeric Media. *J. Chem. Phys.* **1946**, *14* (2), 80−92.

(28) Rubinstein, M.; Semenov, A. N. Thermoreversible Gelation in Solutions of Associating Polymers. 2. Linear Dynamics. *Macromolecules* **1998**, *31* (4), 1386−1397.

(29) Baxandall, L. G. Dynamics of reversibly crosslinked chains. *Macromolecules* **1989**, *22* (4), 1982−1988.
(30) Leibler, L.; Rubinstein, M.; Colby, R. H. Dynamics of reversible networks. *Macromolecules* **1991**, *24* (16), 4701−4707.
(31) Jiang, N.; Zhang, H.; Tang, P.; Yang, Y. Linear Viscoelasticity of Associative Polymers: Sticky Rouse Model and the Role of Bridges. *Macromolecules* **2020**, *53* (9), 3438−3451.
(32) Jiang, N.; Zhang, H.; Yang, Y.; Tang, P. Molecular dynamics simulation of associative polymers: Understanding linear viscoelasticity from the sticky Rouse model. *J. Rheol.* **2021**, *65* (4), 527−547.
(33) Shao, J.; Jiang, N.; Zhang, H.; Yang, Y.; Tang, P. Sticky Rouse Model and Molecular Dynamics Simulation for Dual Polymer Networks. *Macromolecules* **2022**, *55* (2), 535−549.
(34) Hoy, R. S.; Fredrickson, G. H. Thermoreversible associating polymer networks. I. Interplay of thermodynamics, chemical kinetics, and polymer physics. *J. Chem. Phys.* **2009**, *131* (22), 224902.
(35) Wu, J. B.; Li, S. J.; Liu, H.; Qian, H. J.; Lu, Z. Y. Dynamics and reaction kinetics of coarse-grained bulk vitrimers: a molecular dynamics study. *Phys. Chem. Chem. Phys.* **2019**, *21* (24), 13258−13267.
(36) Perego, A.; Lazarenko, D.; Cloitre, M.; Khabaz, F. Microscopic Dynamics and Viscoelasticity of Vitrimers. *Macromolecules* **2022**, *55* (17), 7605−7613.
(37) Perego, A.; Khabaz, F. Volumetric and Rheological Properties of Vitrimers: A Hybrid Molecular Dynamics and Monte Carlo Simulation Study. *Macromolecules* **2020**, *53* (19), 8406−8416.
(38) Xia, J.; Kalow, J. A.; Olvera de la Cruz, M. Structure, Dynamics, and Rheology of Vitrimers. *Macromolecules* **2023**, *56* (19), 8080−8093.
(39) Xia, J.; Olvera de la Cruz, M. Dynamics and Structure of Unentangled Associative Polymers. *Macromolecules* **2024**, 8793.
(40) Sciortino, F. Three-body potential for simulating bond swaps in molecular dynamics. *Eur. Phys. J. E Soft Matter* **2017**, *40* (1), 3.
(41) Ciarella, S.; Sciortino, F.; Ellenbroek, W. G. Dynamics of Vitrimers: Defects as a Highway to Stress Relaxation. *Phys. Rev. Lett.* **2018**, *121* (5), No. 058003.
(42) Ciarella, S.; Biezemans, R. A.; Janssen, L. M. C. Understanding, predicting, and tuning the fragility of vitrimeric polymers. *Proc. Natl. Acad. Sci. U. S. A.* **2019**, *116* (50), 25013−25022.
(43) Ciarella, S.; Ellenbroek, W. G. Bond swaps in molecular dynamics on graphic processing units. *arXiv: Soft Condensed Matter* 2019.
(44) Ciarella, S.; Ellenbroek, W. G. Swap-Driven Self-Adhesion and Healing of Vitrimers. *Coatings* **2019**, *9* (2), 114.
(45) Zhao, H.; Wei, X.; Fang, Y.; Gao, K.; Yue, T.; Zhang, L.; Ganesan, V.; Meng, F.; Liu, J. Molecular Dynamics Simulation of the Structural, Mechanical, and Reprocessing Properties of Vitrimers Based on a Dynamic Covalent Polymer Network. *Macromolecules* **2022**, *55* (4), 1091−1103.
(46) Cui, X.; Jiang, N.; Shao, J.; Zhang, H.; Yang, Y.; Tang, P. Linear and Nonlinear Viscoelasticities of Dissociative and Associative Covalent Adaptable Networks: Discrepancies and Limits. *Macromolecules* **2023**, *56* (3), 772−784.
(47) Zhang, Z.; Huang, C.; Weiss, R. A.; Chen, Q. Association energy in strongly associative polymers. *J. Rheol.* **2017**, *61* (6), 1199−1207.
(48) Watanabe, H.; Matsumiya, Y.; Masubuchi, Y.; Urakawa, O.; Inoue, T. Viscoelastic Relaxation of Rouse Chains undergoing Head-to-Head Association and Dissociation: Motional Coupling through Chemical Equilibrium. *Macromolecules* **2015**, *48* (9), 3014−3030.
(49) Matsumiya, Y.; Watanabe, H.; Urakawa, O.; Inoue, T. Experimental Test for Viscoelastic Relaxation of Polyisoprene Undergoing Monofunctional Head-to-Head Association and Dissociation. *Macromolecules* **2016**, *49* (18), 7088−7095.
(50) Rao, A.; Ramírez, J.; Olsen, B. D. Mechanisms of Self-Diffusion of Linear Associative Polymers Studied by Brownian Dynamics Simulation. *Macromolecules* **2021**, *54* (24), 11212−11227.
(51) Mahmad Rasid, I.; Rao, A.; Holten-Andersen, N.; Olsen, B. D. Self-Diffusion in a Weakly Entangled Associative Network. *Macromolecules* **2022**, *55* (14), 6056−6066.
(52) Wu, S.; Yang, H.; Huang, S.; Chen, Q. Relationship between Reaction Kinetics and Chain Dynamics of Vitrimers Based on Dioxaborolane Metathesis. *Macromolecules* **2020**, *53* (4), 1180−1190.
(53) Wu, S.; Yang, H.; Xu, W.-S.; Chen, Q. Thermodynamics and Reaction Kinetics of Symmetric Vitrimers Based on Dioxaborolane Metathesis. *Macromolecules* **2021**, *54* (14), 6799−6809.
(54) Porath, L. E.; Evans, C. M. Importance of Broad Temperature Windows and Multiple Rheological Approaches for Probing Viscoelasticity and Entropic Elasticity in Vitrimers. *Macromolecules* **2021**, *54* (10), 4782−4791.
(55) Zhao, H.; Duan, P.; Li, Z.; Chen, Q.; Yue, T.; Zhang, L.; Ganesan, V.; Liu, J. Unveiling the Multiscale Dynamics of Polymer Vitrimers Via Molecular Dynamics Simulations. *Macromolecules* **2023**, *56* (23), 9336−9349.
(56) Stukalin, E. B.; Cai, L. H.; Kumar, N. A.; Leibler, L.; Rubinstein, M. Self-Healing of Unentangled Polymer Networks with Reversible Bonds. *Macromolecules* **2013**, *46* (18), 7525.
(57) Brassinne, J.; Cadix, A.; Wilson, J.; van Ruymbeke, E. Dissociating sticker dynamics from chain relaxation in supramolecular polymer networks—The importance of free partner! *J. Rheol.* **2017**, *61* (6), 1123−1134.
(58) Ge, S.; Carden, G. P.; Samanta, S.; Li, B.; Popov, I.; Cao, P.-F.; Sokolov, A. P. Associating Polymers in the Strong Interaction Regime: Validation of the Bond Lifetime Renormalization Model. *Macromolecules* **2023**, *56* (6), 2397−2405.
(59) Shanbhag, S.; Ricarte, R. G. On the Effective Lifetime of Reversible Bonds in Transient Networks. *Macromol. Theory Simul.* **2023**, *32* (4), 2300002.
(60) Gold, B. J.; Hovelmann, C. H.; Luhmann, N.; Szekely, N. K.; Pyckhout-Hintzen, W.; Wischnewski, A.; Richter, D. Importance of Compact Random Walks for the Rheology of Transient Networks. *ACS Macro Lett.* **2017**, *6* (2), 73−77.
(61) Hansen, D. R.; Shen, M. Viscoelastic Retardation Time Computations for Homogeneous Block Copolymers. *Macromolecules* **1975**, *8* (3), 343−348.
(62) Wang, F. W.; DiMarzio, E. A. The Dynamics of Block-Copolymer Molecules in Solution. The Free-Draining Limit. *Macromolecules* **1975**, *8* (3), 356−360.
(63) Stockmayer, W. H.; Kennedy, J. W. Viscoelastic Spectrum of Free-Draining Block Copolymers. *Macromolecules* **1975**, *8* (3), 351−355.
(64) Kremer, K.; Grest, G. S. Dynamics of entangled linear polymer melts: A molecular-dynamics simulation. *J. Chem. Phys.* **1990**, *92* (8), 5057−5086.
(65) Thompson, A. P.; Aktulga, H. M.; Berger, R.; Bolintineanu, D. S.; Brown, W. M.; Crozier, P. S.; in 't Veld, P. J.; Kohlmeyer, A.; Moore, S. G.; Nguyen, T. D.; et al. LAMMPS - a flexible simulation tool for particle-based materials modeling at the atomic, meso, and continuum scales. *Comput. Phys. Commun.* **2022**, *271*, No. 108171.
(66) Ricarte, R. G.; Shanbhag, S. Unentangled Vitrimer Melts: Interplay between Chain Relaxation and Cross-link Exchange Controls Linear Rheology. *Macromolecules* **2021**, *54* (7), 3304−3320.
(67) Ramírez, J.; Sukumaran, S. K.; Vorselaars, B.; Likhtman, A. E. Efficient on the fly calculation of time correlation functions in computer simulations. *J. Chem. Phys.* **2010**, *133* (15), 154103.
(68) Kawasaki, Y.; Watanabe, H.; Uneyama, T. A Note for Kohlrausch-Williams-Watts Relaxation Function. *Nihon Reoroji Gakkaishi* **2011**, *39* (3), 127−131.
(69) Fischer, M.; Heuer, A.; Diddens, D. Structure and Transport Properties of Poly(ethylene oxide)-Based Cross-Linked Polymer Electrolytes—A Molecular Dynamics Simulations Study. *Macromolecules* **2022**, *55* (22), 10229−10242.
(70) Cui, X.; Zhang, L.; Yang, Y.; Tang, P. Understanding the application of covalent adaptable networks in self-repair materials based on molecular simulation. *Soft Matter* **2024**, *20* (7), 1486−1498.

https://doi.org/10.1021/acs.macromol.4c02349
Macromolecules 2025, 58, 1898−1911

(71) Chen, M.; Si, H.; Zhang, H.; Zhou, L.; Wu, Y.; Song, L.; Kang, M.; Zhao, X.-L. The Crucial Role in Controlling the Dynamic Properties of Polyester-Based Epoxy Vitrimers: The Density of Exchangeable Ester Bonds (*v*). *Macromolecules* **2021**, *54* (21), 10110−10117.

https://doi.org/10.1021/acs.macromol.4c02349
Macromolecules 2025, 58, 1898−1911